Photodetectors for silicon photonic integrated circuits

1

Molly Piels and John E. Bowers
Department of Electrical and Computer Engineering, University of California Santa Barbara, Santa Barbara, CA, USA

1.1 Introduction

Silicon-based photonic components are especially attractive for realizing low-cost photonic integrated circuits (PICs) using high-volume manufacturing processes (Heck et al., 2013). Due to its transparency in the telecommunications wavelength bands near 1310 and 1550 nm, silicon is an excellent material for realizing low-loss passive optical components. For the same reason, it is not a strong candidate for sources and detectors, and photodetector fabrication requires the integration of either III/V materials or germanium if high speed and high efficiency are required. Photodetectors used in photonic integrated circuits, like photodetectors used in most other applications, typically require large bandwidth, high efficiency, and low dark current. In addition, the devices must be waveguide-integrated (rather than surface-illuminated) and the process used to fabricate the photodiode must be compatible with the processes used to fabricate other components on the chip. For many applications where PICs are a promising solution, for example microwave frequency generation, coherent receivers, and optical interconnects relying on receiverless circuit designs (Assefa et al., 2010b), the maximum output power is also an important figure of merit.

There are numerous design trade-offs between speed, efficiency, and output power. Designing for high bandwidth favors small devices for low capacitance. Small devices require abrupt absorption profiles for good efficiency, but design for high output power favors large devices with dilute absorption. Most of the work on silicon-based photodiodes to date has focused on PIN diodes. Both ultra-compact devices with abrupt absorption profiles and devices with larger active areas have been demonstrated. The results have been consistent with this trade-off: ultra-compact devices have shown the highest bandwidth-efficiency products (up to 38 GHz (Virot et al., 2013)), while devices utilizing dilute absorption profiles had better power handling (up to 19 dBm output power at 1 GHz (Piels et al., 2013)). Recently, photodetectors with decoupled structures, the separate absorption charge and multiplication (SACM) avalanche structure and the uni-traveling carrier (UTC) structure, have been used in both germanium (Piels and Bowers, 2014; Dai et al., 2010, 2014; Duan et al., 2013) and hybrid III/V-silicon (Beling et al., 2013b) to push performance past the limits imposed by the PIN structure.

Photodetectors.

In this chapter, we will review the status of heterogeneous integration of silicon waveguides and photodetectors. First, we will cover available fabrication technologies (both Ge and hybrid III/V-silicon). We will then discuss the design constraints that are common to all waveguide photodiodes on silicon substrates. We will present an overview of demonstrated devices, and lastly conclude and show an outlook for the future.

1.2 Technology

Waveguide photodiodes on silicon broadly fall into one of two categories: germanium-based and hybrid III/V-silicon. A number of groups have demonstrated Ge-based photodiodes in mature fabrication technology based on a CMOS pilot line (Assefa et al., 2010a; Marris-Morini et al., 2014; Galland et al., 2013). In these works, the photodiodes have been cofabricated with passive optics, modulators, and in some cases transistors, but not optical sources (lasers or LEDs). On the other hand, hybrid or InGaAs-based photodiodes have generally been fabricated using technology that is further from mass-production capabilities, but that has a full library of components (competitive with InP substrate-based devices) available (Koch et al., 2013).

1.2.1 Germanium

Germanium is an appealing absorbing material for use in silicon-based PICs because it can be integrated into a CMOS pilot line relatively easily (Si/Ge alloyed contacts are already used in CMOS electronics) and because the bulk material is absorbing in the entire 1310 nm window and much of the C and L bands. There are a number of ways to integrate germanium and silicon, but selective area growth by chemical vapor deposition is the most common for waveguide photodiodes (Michel et al., 2010). The Si/Ge interface is conductive, and for vertical diodes, one contact is often composed of silicon. A typical geometry is shown in Figure 1.1a. There is a 4% lattice mismatch between germanium and silicon, which is relieved through

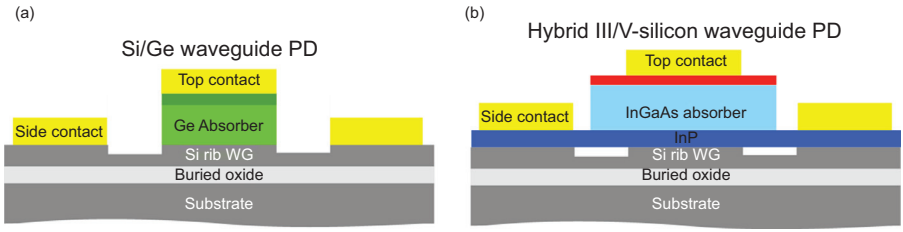

Figure 1.1 Cross-section schematics of waveguide photodiodes on (a) Si/Ge and (b) hybrid III/V-silicon. A vertical diode configuration is shown here, but the diode can also be formed laterally.

the formation of threading defects (Hartmann et al., 2005). These threading defects form mid-gap generation-recombination centers, which increase the dark current of the detector relative to a bulk Ge diode (Mueller, 1959; Giovane et al., 2001). The threading defects also pin the Fermi level in their immediate vicinity, and thus for vertical PIN diodes, the p-down configuration is preferred (Masini et al., 2001).

Germanium epitaxially grown on silicon has superior properties to bulk germanium for a C-band or L-band detector. After growth is completed, as the wafer is cooled from the growth temperature to room temperature, the thermal expansion coefficient mismatch between the two materials results in the formation of tensile strain in the germanium (Liu et al., 2004). This decreases the direct bandgap energy, pushing the direct band edge to around 0.782 eV or lower (1599 nm).

1.2.2 Hybrid III/V-silicon

The hybrid III/V-silicon platform enables the inclusion of optical gain in PICs. The III/V layer stack is usually bonded to the SOI waveguide, but can also be epitaxially grown on Si (Liu et al., 2014). For oxygen plasma enhanced bonding, lattice mismatch does not cause threading defect formation. Thus, any III/V material that can be grown on InP or other III-V substrates, including material with optical gain, can be used in a hybrid III/V-Si PIC. For low temperature oxygen plasma enhanced bonding, the Si/InP interface is not conductive, and both sides of the diode must be in the III/V layers. This results in most devices having the geometry shown in Figure 1.1b. The InP contact layer thickness affects the optical properties of the device, and is typically around 200 nm. For higher temperature bonding, conduction through the interface is possible (Hawkins et al., 1997; Tanabe et al., 2012).

It is possible to use the same epitaxial material for both a laser/amplifier and a photodiode, and this was the approach pursued by the first hybrid III/V-silicon photodiode demonstration (Park et al., 2007). However, in this case, the quantum well depth affects both amplifier performance and photodiode bandwidth, and it is difficult to optimize both simultaneously (Højfeldt and Mørk, 2002). Instead, for applications requiring high bandwidths, InGaAs lattice-matched to InP is the absorbing material of choice. Fabricating hybrid III/V-Si PICs using multiple epitaxial materials is more complex than using a single material (Chang et al., 2010), but has been successfully demonstrated (Koch et al., 2013).

The germanium absorption coefficient in the C and L-bands is a function of growth conditions, but it is typically around 3000 cm^{-1} in the C-band with a long wavelength cutoff around 1600 nm. InGaAs is direct gap and has a larger absorption coefficient in the C-band (around 9600 cm^{-1}), and absorbs well in the entire L-band independent of growth conditions. The real part of the refractive index is relatively low (about 3.6 as opposed to 4.2), which can make designing short, compact devices more difficult in the hybrid platform. However, InP offers greater flexibility in band engineering and optical matching layer design due to the availability of more mature growth technology.

1.2.3 Other technologies

There are a number of other promising technologies for fabricating photodiodes on silicon platforms. Photodiodes based on defect-enhanced absorption in silicon have been demonstrated, and are promising for monitoring purposes (Knights and Doylend, 2008). To move the Ge band edge toward longer wavelengths, Sn has been incorporated in the growth (Roucka et al., 2011), but waveguide-integrated GeSn photodiodes have yet to be demonstrated. InGaAs has been grown epitaxially on (Feng et al., 2012) and fused to (Black et al., 1997) silicon, resulting in a conductive interface. In both cases, the dark current is increased relative to low-temperature bonded and native-substrate material. For optical interconnect applications, InGaAs nanopillars grown on silicon substrates have shown good performance as both photodetectors and optical sources (Chen et al., 2011).

1.3 Optical properties of Si-based WGPDs

There are two commonly used schemes for coupling to a waveguide photodiode: butt-coupling and vertical coupling. In a butt-coupled photodiode, the absorbing region sits in a recess at the end of the input waveguide. Vertically-coupled photodiodes have an absorbing region that lies on top of the input waveguide. The fabrication process for butt-coupled photodiodes is typically more complex than the fabrication of vertically-coupled photodiodes and most practical when the absorbing region is grown, rather than bonded. The primary benefit of the butt-coupled photodiode is that the confinement of the optical mode in the absorbing region is very high, and thus ultra-compact devices with high efficiency and low capacitance can be fabricated. The highest bandwidth-efficiency products for waveguide photodiodes on silicon reported to-date have been for butt-coupled devices (Virot et al., 2013; DeRose et al., 2011). In addition to a less complicated fabrication process, vertically coupled photodiodes typically have a larger active device area. This makes it relatively difficult to achieve high bandwidth and low dark current, but is preferable for applications requiring high saturated output power (e.g., microwave photonics and coherent communications).

Whereas the optical design of butt-coupled detectors is straightforward (Bowers and Burrus, 1986), the optical design of vertically coupled photodetectors on silicon requires careful simulation. Cross-section schematics of both InGaAs and germanium-based waveguide photodiodes are shown in Figure 1.1. In both cases, the absorbing region has a real refractive index that is larger than the real refractive index of silicon, so the fundamental mode in the detector area has low overlap with the input mode from the input passive waveguide. Thus the coupling from the input passive waveguide is typically to higher-order modes in the photodiode area. The absorption profile depends on the confinement factor of the higher-order mode in the absorbing region and the overlap between it and the input mode, both of which are functions of the absorber thickness. The end result is that the absorption profile of the device is a strong function of absorbing region thickness. The efficiency of a

device of a given length displays local maxima and minima, as shown in Figure 1.2a for germanium and Figure 1.2b for InGaAs. The simulation was done using the semi-vectorial beam propagation method for a TE-polarized input.

On both material platforms, the absorption profile also depends on the underlying silicon thickness, waveguide width, input polarization, and wavelength. In the Si/Ge system, the locations of the maxima and minima are roughly the same for both polarizations over large optical bandwidths. Thus devices with low polarization-dependent responsivity and high efficiency over an optical bandwidth in excess of 100 nm have been demonstrated (Yin et al., 2007). On the hybrid III/V-silicon platform, performance is more sensitive to design parameters. This is for a number of reasons, primary among them is that the real part of the refractive index of InGaAs is closer to the real part of the refractive index of Si and the imaginary part is large enough to affect the confinement factor. The drawback of this sensitivity is that optical simulations of hybrid silicon devices require excellent material models in order to accurately predict performance, whereas approximate models often work well for Si/Ge detectors (Piels et al., 2013; Yin et al., 2007).

The absorption characteristics are very important to determining how design trade-offs between efficiency, bandwidth, and output power behave. For some types of waveguide detectors (e.g., butt-coupled), a minor change in absorber thickness will have either no impact or an easily mitigated impact on the absorption profile. The peak/valley behavior in Figure 1.2, on the other hand, means that for vertically coupled waveguide photodiodes on silicon, the optical and the electrical design must be done simultaneously.

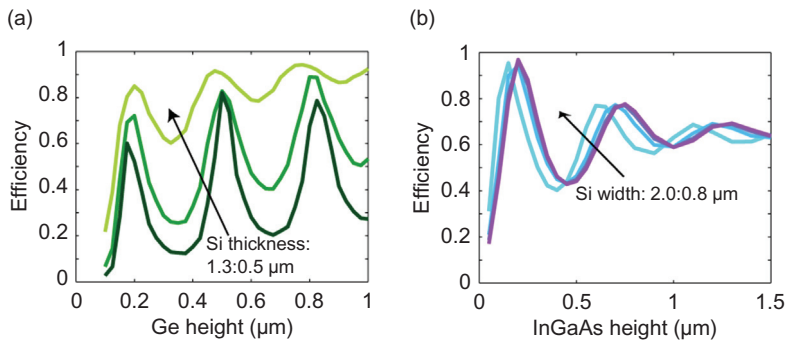

Figure 1.2 Simulated quantum efficiency of a 20 μm-long TE photodetector as a function of (a) Ge thickness and (b) InGaAs thickness for waveguide detectors on silicon. For the Si/Ge photodetector, the underlying silicon thickness is the parameter; the dependence of the absorption profile on width is minimal for easily fabricated device sizes (wider than 2 μm). For the hybrid III/V-Si detector, the parameter is the width of the silicon rib waveguide. The thickness and rib height are assumed to be 500 and 250 nm, respectively, as these dimensions are often used for this kind of device.

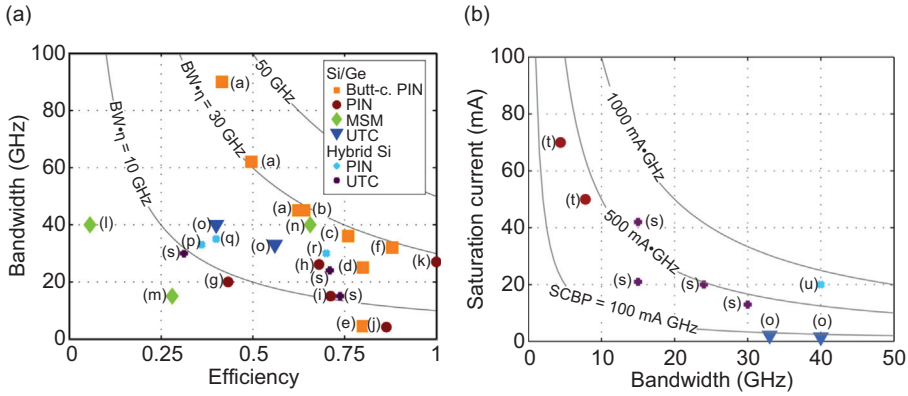

Figure 1.3 (a) Bandwidth-efficiency and (b) output power-bandwidth trade-offs for demonstrated waveguide devices. Devices with avalanche gain are not included in these plots. Contours for bandwidth-efficiency products of 10, 30, and 50 GHz are also shown in (a) and contours for saturation current-bandwidth products of 100, 500, and 1000 mA GHz are shown in (b). a: (Virot et al., 2013), b: (DeRose et al., 2011), c: (Liao et al., 2011), d: (Vivien et al., 2007), e: (Liu et al., 2006) (1520 nm), f: (Feng et al., 2009), g: (Wang et al., 2008; OpSIS), h: (Yin et al., 2007), i: (Masini et al., 2008) (divided optical bandwidth by $\sqrt{3}$), j: (Ahn et al., 2007) (divided optical bandwidth by $\sqrt{3}$), k: (Liow et al., 2013), l: (Assefa et al., 2009), m: (Assefa et al., 2013), n: (Chen and Lipson, 2009) (from pulsed measurement; $f_{3dB} = 0.312\tau_{FWHM}$ (Weingarten et al., 1988)), o: (Piels and Bowers, 2014), p: (Binetti et al., 2010), q: (Lee et al., 2013), r: (Piels et al., 2014), s: (Beling et al., 2013b, t: (Bowers et al., 2010), u: (Ramaswamy, 2014).

1.4 Demonstrated waveguide photodiodes on silicon

This section presents the state of the art on waveguide photodetectors on silicon, organized by cross-section design. Figure 1.3a shows the electrical bandwidth and efficiency of a number of research devices on silicon. Unless otherwise indicated, the efficiency in the figure was measured at 1550 nm. The vertically-coupled PIN designs, represented by red circles for Ge and blue crosses for hybrid silicon, offer ease of fabrication for electrical bandwidths up to 30 GHz. For higher speeds, alternative approaches such as the butt-coupled PIN (orange rectangles), metal-semiconductor-metal (MSM; green diamonds) or UTC photodiode (blue triangles; purple crosses) have been necessary. Figure 1.3b shows the same electrical bandwidth and saturation current (the time-average current at −1 dB power compression) for the same set of devices. All devices shown are vertically-coupled, and the trend illustrates the well-known saturation current-bandwidth trade-off.

1.4.1 Vertically coupled PIN photodiodes in Si/Ge and InGaAs

The PIN diode is one of the most commonly used photodiode cross-section designs. In a PIN detector, most of the light is absorbed in the intrinsic region in the center

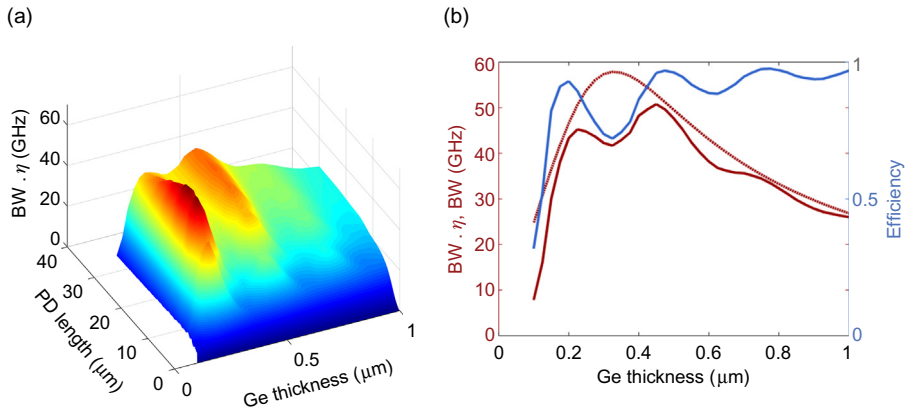

Figure 1.4 (a) Bandwidth-efficiency product for a vertically-coupled Si/Ge PIN photodiode as a function of intrinsic region thickness and device length. The assumed width is 3 μm. (b) Bandwidth, efficiency, and bandwidth-efficiency product for a 30 μm × 3 μm vertically-coupled Si/Ge PIN photodiode as a function of intrinsic region thickness.

of the device. For bandwidth, PIN design involves balancing the RC and the transit time limit. The RC limit is approximately

$$f_{\mathrm{RC}} = \frac{1}{2\pi(R_{\mathrm{s}} + R_{\mathrm{L}})C} \tag{1.1}$$

where R_{s} is the diode series resistance, R_{L} is the load resistance (typically 50 Ω), and C is the diode capacitance, and the transit time limit is about (Bowers and Burrus, 1987)

$$f_{\tau} = \frac{0.45v}{W} \tag{1.2}$$

where v is the smaller of the saturated electron and hole velocities and W is the intrinsic region thickness. Since the diode capacitance is approximately $\varepsilon A/W$, where A is the diode area, there is an optimum intrinsic region thickness.

For vertically-coupled PIN photodiodes, the highest bandwidth-efficiency products can be obtained by choosing an absorption region thickness at a peak in Figure 1.2. This is shown for a Si/Ge PIN as a surface plot in Figure 1.4a. The calculation includes the transit time and RC limits assuming a 50 Ω load, but neglects parasitic effects. The capacitance was calculated using a parallel plate model and a device width of 3 μm. The germanium region was assumed to be completely depleted for both bandwidth estimates (i.e., the thicknesses of the p- and n-contact were assumed negligible or had negligible absorption due to larger bandgap contact layers). The silicon waveguide height was 500 nm. The maximum values of bandwidth-efficiency product in Figure 1.4a are limited to below

60 GHz because the optimum thicknesses for fast absorption do not necessarily correspond to thicknesses where the RC and transit time constants have been carefully balanced. This is shown (under the same assumptions used in Figure 1.4a) in Figure 1.4b for a 30 μm long device. For maximum bandwidth, the optimum germanium region thickness is 300 nm, but for maximum efficiency, 200 and 400 nm give better performance.

Despite these difficulties, several devices with good performance have been demonstrated. The largest demonstrated bandwidth of a vertically-coupled PIN photodiode on Si/Ge is 27 GHz (Liow et al., 2013). Two Intel NIP photodiodes (Yin et al., 2007) had responsivities of 0.89 and 1.16 A/W at 1550 nm and electrical bandwidths of 26 and 24.1 GHz. A Luxtera device performed similarly, with a responsivity of 0.85 A/W and bandwidth of 26 GHz (Masini et al., 2008). Finally, IME demonstrated photodetectors with a 20 GHz bandwidth and 0.54 A/W responsivity (Wang et al., 2008; OpSIS). The same group has recently demonstrated detectors with improved responsivity and the same bandwidth using (low-field) avalanche multiplication (Liow et al., 2013), and extended the 3 dB bandwidth by using inductive gain peaking (Novack et al., 2013). It has proven difficult to increase the bandwidth of a vertically coupled germanium PIN beyond 30 GHz in a 50 Ω environment while maintaining high efficiency.

The design space and results for hybrid III/V-silicon PIN photodetectors are similar to those for Si/Ge photodetectors. Optically, although the absorption profile can be altered by changing the width of the underlying silicon, achieving a large change in confinement factor requires a very narrow waveguide, which in turn requires lithography with higher resolution than what has historically been used to fabricate this kind of device. Electrically, the transit time-limited bandwidth of an InGaAs-based PIN detector is slightly lower and the RC-limited bandwidth is slightly higher than the same quantities for an equivalent Si/Ge PIN. This is because the hole velocity in InGaAs is slower than the carrier velocities in Ge, increasing the transit time, and the dielectric constant is lower, which decreases the capacitance. The performance of demonstrated devices is also similar to the performance of Si/Ge PINs; a number of different devices have been demonstrated, and the bandwidths were all around 30 GHz (Binetti et al., 2010; Lee et al., 2013; Piels et al., 2014; Ramaswamy, 2014).

Both Si/Ge and hybrid III/V-silicon PIN detectors have been investigated for use in high-power applications. The main limitations on output power are the active area of the device and the maximum current density the cross-section can sustain before the internal field collapses (Williams and Esman, 1999). In the intrinsic region of a photodetector, under low-injection conditions, there is a roughly constant electric field due to the applied bias that separates the charge carriers. As the current density in the intrinsic region increases, the carriers screen the electric field. Under high injection, the field distribution redistributes with the minimum occurring in the intrinsic region. The maximum current density is reached when the minimum of the electric field drops below the value necessary for the carriers to be able to maintain their saturation velocities. For a PIN photodetector, this can be expressed as (Piels, 2013)

$$J_{max} = \frac{6\varepsilon v_n v_p}{W^2(v_n + v_p)}(V_{bi} + V_{PD} - E_{crit}W) \tag{1.3}$$

where ε is the dielectric constant of the intrinsic region, v_n and v_p are the saturated electron and hole velocities, W is the intrinsic region width, V_{bi} is the diode built-in voltage, V_{PD} is the voltage drop across the device due to the load resistance and applied bias, and E_{crit} is the electric field at which the carrier velocities saturate. The factor $6\varepsilon v_n v_p / W_i^2(v_n + v_p)$ determines how the saturation current scales with bias voltage, and should be as large as possible for high-power conversion efficiency (Tulchinsky et al., 2008). In germanium, it is $2.6e-5$ A/V/cm^2, while for InGaAs it is $2.3e-5$ A/V/cm^2, and so we expect slightly better power handling from a Si/Ge PIN than from an InGaAs PIN with the same dimensions at the same bias voltage. However, the breakdown field of InGaAs is about twice that of Ge, so in the absence of a system limit on bias voltage (and neglecting thermal effects), the InGaAs device would have a larger saturated output power.

1.4.2 Butt-coupled PIN photodiodes in Ge

One approach to increasing the bandwidth beyond 30 GHz is to use a butt-coupled or nearly butt-coupled design (Virot et al., 2013; DeRose et al., 2011; Liao et al., 2011; Vivien et al., 2007; Feng et al., 2009). The confinement factor in the germanium for these photodiodes is nearly 100% regardless of the total germanium thickness used. As a result, most of the light can be absorbed by very short (less than 10 μm long) devices. The highest bandwidths for waveguide photodiodes on silicon to date have been reported for ultra-compact butt-coupled PIN detectors.

The optical characteristics of the device are relatively insensitive to the germanium thickness and device width, so a large degree of electrical optimization is possible. Due to their small size, the capacitance of ultra-compact devices is usually very small, regardless of the intrinsic region thickness. This enables the use of very thin intrinsic regions for decreased transit time and operating voltage. There is a significant fabrication challenge in getting the contact resistance low enough for high bandwidth in a 50 Ω environment, but in large part these are being advocated for applications where a larger series resistance may be acceptable. The primary disadvantage of such ultra-compact designs comes in power handling. Due to the small active device area, the maximum output power is expected to be low.

1.4.3 MSM photodetectors

Another way to increase the bandwidth is to use a cross-section design with lower capacitance per unit area. MSM detectors have this property, and have been demonstrated on Si/Ge. IBM successfully integrated a germanium-based photodiode with a 38 GHz bandwidth into a CMOS process flow, though the responsivity at 1550 nm was only 0.07 A/W (Assefa et al., 2009). The same group integrated similar devices with higher responsivity and lower bandwidth with TIAs (Assefa et al.,

2013). They also showed that it is possible to use such a structure in avalanche mode at low (1.5 V) bias, which yields a significant sensitivity improvement, while maintaining a 30 GHz bandwidth (Assefa et al., 2010c). Chen and Lipson demonstrated a device with 40 GHz bandwidth and higher (0.35 A/W) responsivity fabricated using wafer-bonding (Chen and Lipson, 2009). For both devices, because the germanium is not grown on silicon using CVD, the responsivity begins to roll off at relatively short wavelengths. In general, MSM devices can have lower capacitance per unit area than PIN detectors because the depletion region only occupies a fraction of the device area. One consequence of this is that the saturation current density is also decreased. In addition, the dark current of MSM detectors is often higher than the dark current of PIN diode-based devices.

1.4.4 SACM avalanche photodiodes

For the lowest noise receivers, photodetectors with gain are attractive, using either avalanche or photoconductive gain. Silicon is an excellent material for avalanche gain due to the low electron and hole ionization coefficient ratio ($k < 0.1$), which allows for high gain-bandwidth products and low excess noise factors. SACM avalanche photodetectors (APDs) using silicon avalanche regions have been demonstrated using both III-V (Hawkins et al., 1997) and Ge (Dai et al., 2010) absorbing regions. In the surface-normal configuration, gain-bandwidth products up to 840 GHz (Sfar Zaoui et al., 2009) have been demonstrated in for Si/Ge devices and up to 315 GHz (Hawkins et al., 1997) have been demonstrated for III-V/Si ones. As waveguide detectors, the highest gain-bandwidth product was at least 380 GHz (Duan et al., 2013) (20 GHz, gain > 19).

1.4.5 Si/Ge UTC photodiodes

The UTC cross-section is an alternative way to push the bandwidth of a waveguide Si/Ge photodiode beyond 30 GHz in a vertically-coupled configuration without decreasing the active device area. A UTC is a decoupled structure where the absorption occurs in a doped layer and carriers are collected through a depleted layer in the silicon. As a result, the germanium thickness can be chosen for optimal coupling from the silicon waveguide without affecting the capacitance, and vertically-coupled devices with relatively large footprints and fast transit times can be fabricated without sacrificing RC performance. Recently, Si/Ge UTCs with a bandwidth of 40 GHz and responsivity of 0.5 A/W have been demonstrated (Piels and Bowers, 2014).

The cross-section and band diagram of the devices in Piels and Bowers (2014) are shown in Figure 1.5. The transit time is dominated by minority electron transport through the absorber and collector (holes in the absorber move to screen the minority charges), which is the origin of the term *uni-traveling* (Ishibashi et al., 1997). In the absorber, photogenerated carriers move toward the collector by a combination of diffusion and drift; the absorber is doped on a grade to produce a small electric field and decrease the transit time. In the collector, injected minority

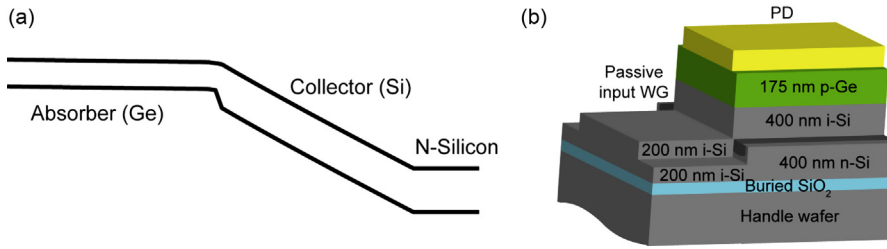

Figure 1.5 (a) Band diagram and (b) cross-section schematic of a waveguide Si/Ge uni-traveling carrier photodetector.
Source: Reprinted with permission from Piels and Bowers (2014).

electrons form a drift current (from the electric field due to the bias voltage) and are collected at the n-contact. Unlike PIN diodes in Si/Ge, UTC detectors perform better when they are p-side up. The threading defects that form at the Si/Ge hetero-interface pin the Fermi level in that region, but if the germanium is doped sufficiently highly, this does not result in the formation of a large barrier (Piels and Bowers, 2014).

UTC photodiodes were first demonstrated in III/V materials, where they have been shown to have superior bandwidth and power handling due to the large electron velocity in InP relative to the hole velocity. In group IV materials, electron and hole velocities are similar, and the benefit of the UTC is instead that it allows us to choose a capacitance per unit area independently from the absorbing region thickness. For the absorption peak at 200 nm Ge thickness, this results in a higher bandwidth-efficiency product. In a UTC photodiode, the transit time is dominated by the electron transport properties and the capacitance is dominated by the collector thickness. The material constants in Eqs (1.1) and (1.2) change, and Eq. (1.3) becomes (Mishra and Singh, 2008)

$$J_{\max} = \frac{2\varepsilon v_n}{W^2}(V_{bi} + V_{PD} - E_{crit}W) \tag{1.4}$$

where ε now refers to the dielectric constant of the silicon collector and W is its thickness.

Figure 1.6a shows idealized design curves for bandwidth and efficiency for PIN and UTC photodiodes assuming a 200 nm thick absorber and a 3 μm wide mesa. Parasitic effects (e.g., pad capacitance and diode series resistance) are neglected in the simulation. The collector thickness of the UTC was chosen separately for each detector length to maximize the bandwidth-efficiency product. As the figure shows, for even moderate efficiency, the UTC out-performs the PIN. Figure 1.6b shows the calculated saturation current-bandwidth product for 3 μm × 30 μm PIN and UTC photodiodes as a function of intrinsic region thickness (Ge for the PIN, Si for the UTC). The assumed bias voltage is half the breakdown voltage of the diode, and the illumination profile was assumed uniform (this will result in an optimistic

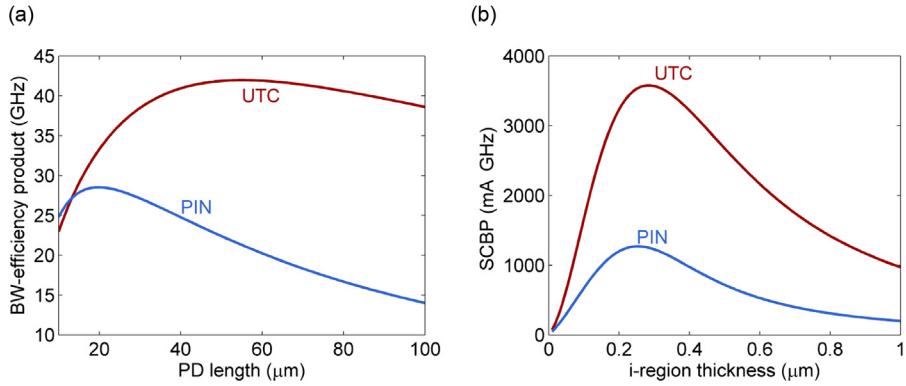

Figure 1.6 (a) BW-efficiency product and (b) saturation current-bandwidth product (SCBP) for ideal PIN and UTC photodiodes assuming 200 nm Ge thickness and a 3 μm wide mesa.

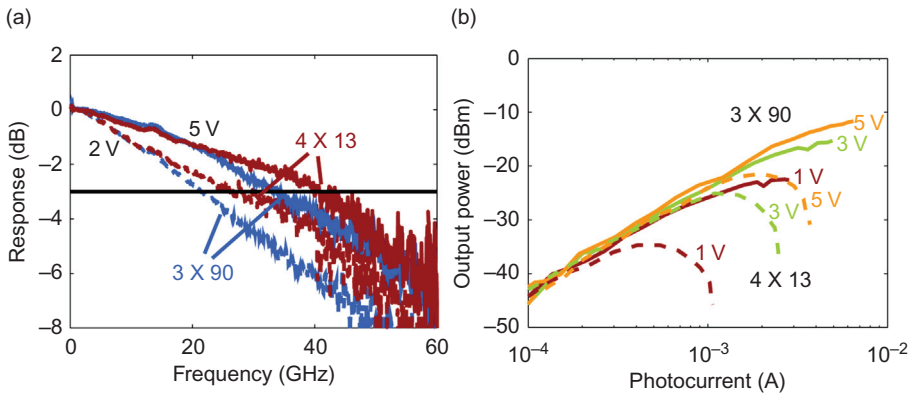

Figure 1.7 (a) Bandwidth and (b) power handling of Si/Ge UTC photodetectors at 30 GHz. *Source*: Reprinted with permission from Piels and Bowers (2014).

estimate of the saturation current). Parasitic effects were again ignored. The UTC has both higher saturation current and higher bandwidth, which leads to higher estimated saturation-current bandwidth products.

In Piels and Bowers (2014), high-speed (>33 GHz) waveguide-type Ge/Si UTC photodiodes with dilute absorption profiles were demonstrated with high responsivities (>0.5 A/W) and high 1 dB-compression (>1.5 mA). Figure 1.7a shows the frequency responses of a 3 μm × 90 μm and a 4 μm × 13 μm device at −2 and −5 V bias. The frequency response was measured with an Agilent lightwave component analyzer at 1550 nm and includes the effect of the probe pad impedance. At −5 V bias, the 3 dB electrical bandwidth of the 3 μm × 90 μm detector was 33 GHz while for the 4 μm × 13 μm detector, it was 40 GHz. The corresponding optical bandwidths (i.e., $10\log_{10}(S_{21})$) of the two devices are 54 and 56 GHz, respectively.

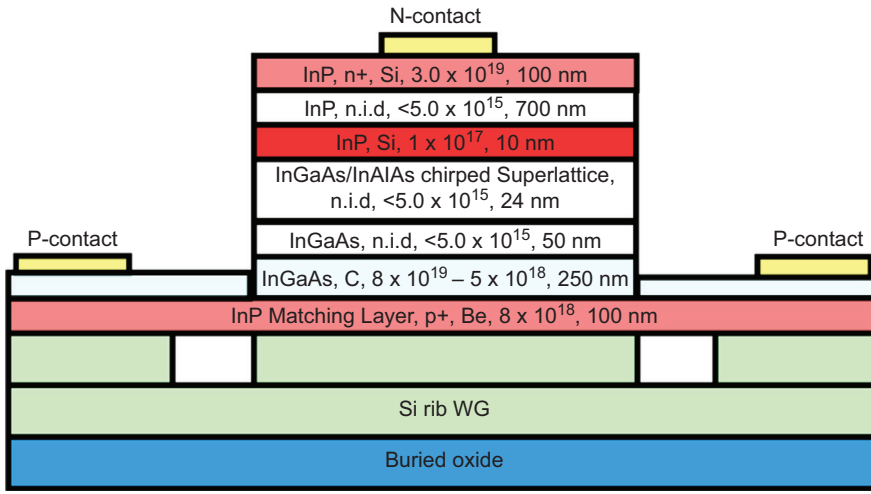

Figure 1.8 Layer stack and cross-section schematic of the hybrid III/V-silicon MUTC photodiode. Doping concentrations are in cm^{-3}.
Source: Reprinted with permission from Beling et al. (2013a).

The large-signal saturation characteristics of the 40 GHz 4 μm × 13 μm and the 33 GHz 3 μm × 90 μm devices discussed above are shown in Figure 1.7b. An 80% modulation depth tone fixed at 30 GHz was generated using the standard heterodyne technique with two free-running lasers at 1537 nm. The RF power was measured on an electrical spectrum analyzer. The loss of the cables was measured with a network analyzer and subtracted from the data. In both cases, the −1 dB compression current is around 2 mA, which corresponds to an output power around −20 dBm. However, the longer device has larger maximum output power since the output power continues to increase after the −1 dB compression current is reached. This is because the back of the device continues to operate in the linear regime even when the front of the device is compressed, whereas for the shorter device, the current is more uniformly distributed. This leads to a sharp decrease in output power beyond the −1 dB compression current for the shorter device, in contrast to a slow increase in output power for the longer one. The maximum output power of the 4 μm × 13 μm detector at 30 GHz is −21.4 dBm, while it is −11.7 dBm for the longer one. Si/Ge UTCs are thus promising for use in high-power high-speed applications. At present, the primary limitation to both bandwidth and power handling is carrier transport through the heterojunction; improved performance can be expected as the growth technology matures.

1.4.6 Hybrid III/V-silicon UTC photodiodes

UTC designs can also be used to increase the bandwidth and output power of hybrid III/V-silicon photodiodes. Figure 1.8 shows a cross-section of a fabricated

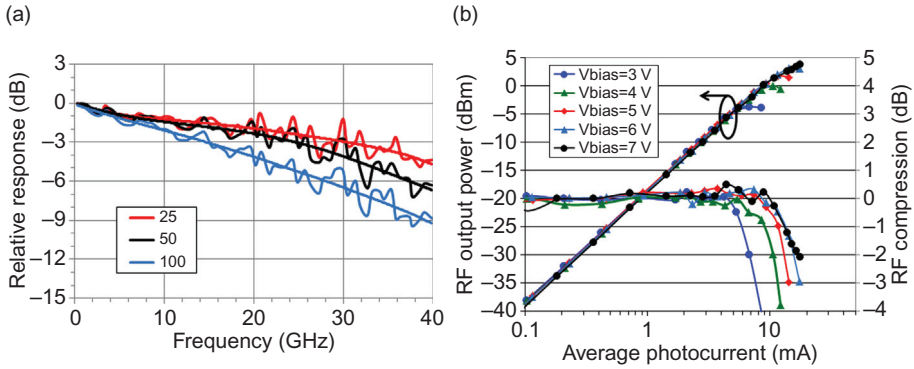

Figure 1.9 (a) Bandwidth and (b) RF output power for hybrid III/V-silicon modified UTCs. *Source*: Reprinted with permission from Beling et al. (2013a).

device (Beling et al., 2013b); it is based on a surface-normal structure that had high bandwidth and high saturated output power (Li et al., 2011). The modified uni-traveling carrier (MUTC) differs from the UTC in that part of the absorbing region closest to the collector is left undoped. The bias voltage thus induces an electric field in the area of the heterojunction, which improves the carrier transport properties, increasing linearity and bandwidth. The ability to do band engineering is a strong difference between the hybrid III/V-Si platform and Si/Ge platform, and we see much better performance for HSP UTCs than for Si/Ge UTCs.

Beling et al. (2013a,b) report on high-speed high-power waveguide MUTC PDs on the hybrid silicon platform with internal responsivities up to 0.85 A/W. Figure 1.9a shows the measured bandwidths of three devices with different lengths (25, 50, and 100 μm) and a 14 μm wide mesa. The bandwidth was measured using an optical heterodyne setup with a modulation depth close to 100%. For the shortest (25 μm) device, the 3 dB bandwidth was 30 GHz. Figure 1.9b shows the RF output power and compression of this device as a function of time-average photocurrent for the shortest device at 30 GHz. The maximum at 30 GHz was 3.9 dBm, while at 20 GHz it was 5.6 dBm.

To increase the RF output power, photodiode arrays were designed and fabricated. Optically, the input was distributed to multiple diodes via a multimode interferometer as shown in Figure 1.10a. Electrically, the signals were summed in parallel at the probe pads. At 20 GHz, a two-photodiode array achieved an RF output power of 9.3 dBm, while a four-detector array achieved an RF output power of 10.2 dBm. The performance was limited by the available input power; in principle, higher output power is possible. For both arrays, the RF output power exceeded that of the single photodiodes discussed above, which indicates the promise of this approach for increasing the output power available from a PIC.

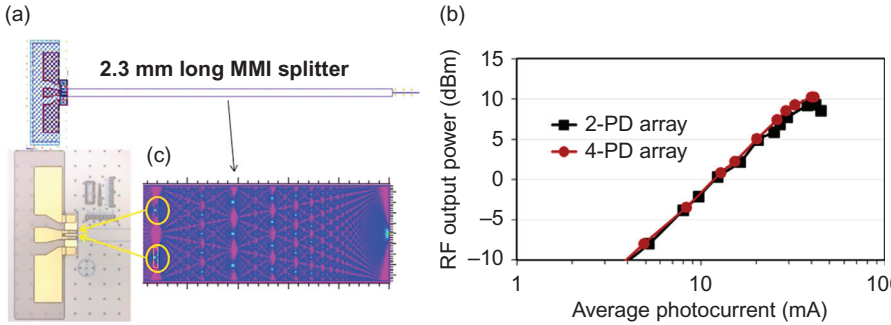

Figure 1.10 MMI-fed photodiode array (a) operating principle and (b) RF output power at 20 GHz as a function of average photocurrent for arrays of 10 μm × 37 μm photodetectors. *Source*: Reprinted with permission from Beling et al. (2013a).

1.5 Conclusions and future outlook

We have presented an overview of photodetectors heterogeneously integrated on silicon-on-insulator. For very high-speed applications where output power is not of great concern, ultra-compact butt-coupled Si/Ge PINs have the best bandwidth and efficiency. For microwave photonics and coherent communication applications requiring large photocurrents, vertically-coupled UTC detectors, either on the hybrid III/V-silicon platform or in Si/Ge, are preferable. Both of these technologies are in their initial stages of development, and can be further improved. The band engineering currently available in III/V (that has been critical to enhancing III/V MUTC performance) can be applied to the Si/Ge UTC as germanium-on-silicon growth technology matures. Advanced optical designs (Beling et al., 2013a,b) can be applied to both platforms, further increasing output power.

References

Ahn, D., Hong, C.-Y., Liu, J., Giziewicz, W., Beals, M., Kimerling, L.C., et al., 2007. High performance, waveguide integrated Ge photodetectors. Opt. Express. 15 (7), 3916–3921.

Assefa, S., Xia, F., Bedell, S.W., Zhang, Y., Topuria, T., Rice, P.M., et al., 2009. CMOS-integrated 40 GHz germanium waveguide photodetector for on-chip optical interconnects. In: Optical Fiber Communication Conference and National Fiber Optic Engineers Conference, San Diego, CA.

Assefa, S., Xia, F., Bedell, S.W., Zhang, Y., Topuria, T., Rice, P.M., et al., 2010a. CMOS-integrated high-speed MSM germanium waveguide photodetector. Opt. Express. 18 (5), 4986–4999.

Assefa, S., Xia, F., Green, W., Schow, C., Rylyakov, A., Vlasov, Y., 2010b. CMOS-integrated optical receivers for on-chip interconnects. IEEE J. Sel. Top. Quantum Electron. 16 (5), 1376–1385.

Assefa, S., Xia, F., Vlasov, Y.A., 2010c. Reinventing germanium avalanche photodetector for nanophotonic on-chip optical interconnects. Nature. 464, 80–84.

Assefa, S., Pan, H., Shank, S., Green, W., Rylyakov, A., Schow, C., et al., 2013. Monolithically integrated silicon nanophotonics receiver in 90 nm CMOS technology node. In: Optical Fiber Communication Conference/National Fiber Optic Engineers Conference, Anaheim, CA.

Beling, A., Cross, A.S., Piels, M., Peters, J., Fu, Y., Zhou, Q., et al., 2013a. High-power high-speed waveguide photodiodes and photodiode arrays heterogeneously integrated on silicon-on-insulator. In: Optical Fiber Communication Conference/National Fiber Optic Engineers Conference, Anaheim, CA.

Beling, A., Cross, A., Piels, M., Peters, J., Zhou, Q., Bowers, J., et al., 2013b. InP-based waveguide photodiodes heterogeneously integrated on silicon-on-insulator for photonic microwave generation. Opt. Express. 21 (22), 25901–25906.

Binetti, P., Leitjens, X.J.M., de Vries, T., Oei, Y.S., Di Cioccio, L., Fédéli, J.M., et al., 2010. InP/InGaAs photodetector on SOI photonic circuitry. IEEE Photonics J. 2 (3), 299–305.

Black, A., Hawkins, A.R., Margalit, N.M., Babic, D.I., Holmes Jr., A.L., Chang, Y.-L., et al., 1997. Wafer fusion: materials issues and device results. IEEE J. Sel. Top. Quantum Electron. 3 (3), 943–951.

Bowers, J.E., Burrus, C.A., 1986. High speed zero bias waveguide photodetectors. Electron. Lett. 22 (17), 905.

Bowers, J.E., Burrus, C., 1987. Ultrawide-band long-wavelength p-i-n photodetectors. J. Lightwave Technol. LT-5 (10), 1339–1350.

Bowers, J.E., Piels, M., Ramaswamy, A., Yin, T., 2010. High power waveguide Ge/Si photodiodes. In: Annual Meeting of the Electrochemical Society, Las Vegas, NV.

Chang, H., Kuo, Y., Jones, R., Barkai, A., Bowers, J.E., 2010. Integrated hybrid silicon triplexer. Opt. Express. 18 (23), 23891–23899.

Chen, L., Lipson, M., 2009. Ultra-low capacitance and high speed germanium photodetectors on silicon. Opt. Express. 17 (10), 7901–7906.

Chen, R., Tran, T.-T.D., Ng, K.W., Ko, S.W., Chuang, L.C., Sedgwick, F.G., et al., 2011. Nanolasers grown on silicon. Nat. Photonics. 5, 170–175.

Dai, D., Chen, H.-W., Bowers, J.E., Kang, Y., Morse, M., Paniccia, M., 2010. Equivalent circuit model of a waveguide-type Ge/Si avalanche photodetector. Phys. Status Solidi C. 7 (10), 2532–2535.

Dai, D., Piels, M., Bowers, J.E., 2014. Monolithic Germanium/Silicon photodetectors with decoupled structures: resonant APDs and UTC photodiodes. J. Sel. Top. Quantum Electron. 20 (6), 3802214.

DeRose, C.T., Trotter, D.C., Zortman, W.A., Starbuck, A.L., Fisher, M., Watts, M.R., et al., 2011. Ultra compact 45 GHz CMOS compatible germanium waveguide photodiode with low dark current. Opt. Express. 19 (25), 24897–24904.

Duan, N., Liow, T.-Y., Lim, A., Ding, L., Lo, G., 2013. High speed waveguide-integrated Ge/Si avalanche photodetector. In: Optical Fiber Communication Conference, Anaheim, CA, United States.

Feng, D., Liao, S., Dong, P., Feng, N.-N., Liang, H., Zheng, D., et al., 2009. High-speed Ge photodetector monolithically integrated with large cross-section silicon-on-insulator waveguide. Appl. Phys. Lett. 95 (26), 261105–261105-3.

Feng, S., Geng, Y., Lau, K.M., Poon, A.W., 2012. Epitaxial III-V-on-silicon waveguide butt-coupled photodetectors. Opt. Lett. 37 (19), 4035–4037.

Galland, C., Novack, A., Liu, Y., Ding, R., Gould, M., Baehr-Jones, T., et al., 2013. A CMOS-compatible silicon photonic platform for high-speed integrated opto-electronics, 87670G-1. Proc. SPIE, 8767.

Giovane, L.M., Luan, H.-C., Agarwal, A., Kimerling, L.C., 2001. Correlation between leakage current density and threading dislocation density in SiGe p-i-n diodes grown on relaxed graded buffer layers. Appl. Phys. Lett. 78, 541–543.

Hartmann, J., Damlencourt, J.-F., Bogumilowicz, Y., Holliger, P., Rolland, G., Billon, T., 2005. Reduced pressure-chemical vapor deposition of intrinsic and doped Ge layers on Si(001) for microelectronics and optoelectronics purposes. J. Cryst. Growth. 274 (1–2), 90–99.

Hawkins, A.R., Wu, W., Abraham, P., Streubel, K., Bowers, J.E., 1997. High gain-bandwidth-product silicon heterointerface photodetector. Appl. Phys. Lett. 70, 303–305.

Heck, M.J.R., Bauters, J.F., Davenport, M.L., Doylend, J.K., Jain, S., Kurczveil, G., et al., 2013. Hybrid silicon photonic integrated circuit technology. IEEE J. Sel Top. Quantum Electron. 19 (4), 6100117.

Højfeldt, S., Mørk, J., 2002. Modeling of carrier dynamics in quantum-well electroabsorption modulators. IEEE J. Sel. Top. Quantum Electron. 8 (6), 1265–1276.

Ishibashi, T., Shimizu, N., Kodama, S., Ito, H., Nagatsuma, T., Furuta, T., 1997. Uni-traveling-carrier photodiodes. In: Ultrafast Electronics and Optoelectronics, Incline Village, NV.

Knights, A.P., Doylend, J.K., 2008. Silicon photonics – recent advances in device development. Advances in Information Optics and Photonics. SPIE Press, pp. 633–656.

Koch, B., Norberg, E., Kim, B., Hutchinson, J., Shin, J., Fish, G., et al., 2013. Integrated silicon photonic laser sources for telecom and datacom. In: Optical Fiber Communication Conference/National Fiber Optic Engineers Conference, Anaheim, CA.

Lee, B., Rylyakov, A., Proesel, J., Baks, C., Rimolo-Donadio, R., Schow, C., et al., 2013. 60-Gb/s receiver employing heterogeneously integrated silicon waveguide coupled photodetector. In: CLEO: 2013 Postdeadline, San Jose, CA.

Li, Z., Fu, Y., Piels, M., Pan, H., Beling, A., Bowers, J.E., et al., 2011. High-power high-linearity flip-chip bonded modified uni-traveling carrier photodiode. Opt. Express. 19 (26), B385–B390.

Liao, S., Feng, N.-N., Feng, D., Dong, P., Shafiiha, R., Kung, C.-C., et al., 2011. 36 GHz submicron silicon waveguide germanium photodetector. Opt. Express. 19 (11), 10967–10972.

Liow, T.-Y., Lim, A.E., Duan, N., Yu, M., Lo, G., 2013. Waveguide germanium photodetector with high bandwidth and high L-band responsivity. In: Optical Fiber Communication Conference/National Fiber Optic Engineers Conference, Anaheim, CA.

Liu, J., Cannon, D.D., Wada, K., Ishikawa, Y., Danielson, D.T., Jongthammanurak, S., et al., 2004. Deformation potential constants of biaxially tensile stressed Ge epitaxial films on Si(100). Phys. Rev. B. 70 (15), 155309.

Liu, J., Ahn, D., Hong, C.Y., Pan, D., Jongthammanurak, S., Beals, M., et al., 2006. Waveguide integrated Ge p-i-n photodetectors on a silicon-oninsulator platform. In: Optics Valley of China International Symposium on Optoelectronics.

Liu, A.Y., Zhang, C., Norman, J., Snyder, A., Lubyshev, D., Fastenau, J.M., et al., 2014. High performance continuous wave 1.3 μm quantum dot lasers on silicon. Appl. Phys. Lett. 104, 041104.

Marris-Morini, D., Virot, L., Baudot, C., Fédéli, J., Rasigade, G., Perez-Galacho, D., et al., 2014. A 40 Gbit/s optical link on a 300-mm silicon platform. Opt. Express. 22 (6), 6674–6679.

Masini, C., Colace, L., Assanto, G., Luan, H.-C., Kimerling, L.C., 2001. High performance p-i-n Ge on Si photodetectors for the near infrared: from model to demonstration. IEEE Trans. Electron Devices. 48 (6), 1092–1096.

Masini, G., Sahni, S., Capellini, G., Witzens, J., Gunn, C., 2008. High-speed near infrared optical receivers based on Ge waveguide photodetectors integrated in a CMOS process. Adv. Opt. Technol. 2008, 196572.

Michel, J., Liu, J., Kimerling, L.C., 2010. High-performance Ge-on-Si photodetectors. Nat. Photonics. 4 (8), 527–534.
Mishra, U.K., Singh, J., 2008. Semiconductor Device Physics and Design. Springer-Verlag, AA Dordrecht, the Netherlands.
Mueller, R.K., 1959. Dislocation acceptor levels in germanium. J. Appl. Phys. 30 (12), 2015–2016.
Novack, A., Gould, M., Yang, Y., Xuan, Z., Streshinsky, M., Liu, Y., et al., 2013. Germanium photodetector with 60 GHz bandwidth using inductive gain peaking. Opt. Express. 21 (23), 28387–28393.
OpSIS, OpSIS-IME O150 process performance summary.
Park, H., Fang, A., Jones, R., Cohen, O., Raday, O., Sysak, M., et al., 2007. A hybrid AlGaInAs-silicon evanescent waveguide photodetector. Opt. Express. 15 (6), 6044–6052.
Piels, M., 2013. Si/Ge Photodiodes for Coherent and Analog Communication. University of California, Santa Barbara, CA.
Piels, M., Bowers, J., 2014. 40 GHz Si/Ge uni-traveling carrier waveguide photodiode. J. Lightwave Technol. 32 (20), 3502–3508.
Piels, M., Ramaswamy, A., Bowers, J., 2013. Nonlinear modeling of waveguide photodetectors. Opt. Express. 21, 15634–15644.
Piels, M., Bauters, J.F., Davenport, M.L., Heck, M.J.R., Bowers, J.E., 2014. Low-loss silicon nitride AWG demultiplexer heterogeneously integrated with hybrid III-V/Silicon photodetectors. J. Lightwave Technol. 32 (4), 817–823.
Ramaswamy, A., 2014. Private communication.
Roucka, R., Mathews, J., Weng, C., Beeler, R., Tolle, J., Menéndez, J., et al., 2011. Development of high performance near IR photodiodes: a novel chemistry based approach to Ge-Sn devices integrated on silicon. IEEE J. Quantum Electron. 47 (2), 213–222.
Sfar Zaoui, W., Chen, H.-W., Bowers, J.E., Bowers, J.E., Kang, Y., Morse, M., et al., 2009. Frequency response and bandwidth enhancement in Ge/Si avalanche photodiodes with over 840 GHz gain-bandwidth-product. Opt. Express. 17 (15), .
Tanabe, K., Watanabe, K., Arakawa, Y., 2012. III-V/Si hybrid photonic devices by direct fusion bonding. Sci. Rep. 2, 349.
Tulchinsky, D.A., Boos, J.B., Park, D., Goetz, P.G., Rabinovich, W.S., Williams, K.J., 2008. High-current photodetectors as efficient, linear, and high-power RF output stages. J. Lightwave Technol. 26 (4), 408–416.
Virot, L., Vivien, L., Fédéli, J., Bogumilowicz, Y., Hartmann, J., Boeuf, F., et al., 2013. High-performance waveguide-integrated germanium PIN photodiodes for optical communication applications. Photonics Res. 1, 140–147.
Vivien, L., Rouviere, M., Fédéli, J.-M., Marris-Morini, D., Damlencourt, J.F., Mangeney, J., et al., 2007. High speed and high responsivity germanium photodetector integrated in a silicon-on-insulator microwaveguide. Opt. Express. 15 (15), 9843–9848.
Wang, J., Loh, W.-Y., Chua, K., Zhang, H., Xiong, Y., Loh, T.H., et al., 2008. Evanescent-coupled Ge p-i-n photodetectors on Si-waveguide with SEG-Ge and comparative study of lateral and vertical p-i-n configurations. IEEE Electron Device Lett. 29 (5), 445–448.
Weingarten, K., Rodwell, M., Bloom, D., 1988. Picosecond optical sampling of GaAs integrated circuits. IEEE J. Quantum Electron. 24 (2), 198–220.
Williams, K.J., Esman, R., 1999. Design considerations for high-current photodetectors. J. Lightwave Technol. 17 (8), 1443–1454.
Yin, T., Cohen, R., Morse, M.M., Sarid, G., Chetrit, Y., Rubin, D., et al., 2007. 31 GHz Ge n-i-p waveguide photodetectors on silicon-on-insulator substrate. Opt. Express. 15 (21), 13965–13971.